Catalysis Today 151 (2010) 304–313

Contents lists available at ScienceDirect

Catalysis Today

journal homepage: www.elsevier.com/locate/cattod

Catalyst size and morphological effects on the interaction of NO_2 with $BaO/\gamma\text{-}Al_2O_3$ materials

Donghai Mei [a,*], Ja Hun Kwak [a], Janos Szanyi [a], Qingfeng Ge [b], Charles H.F. Peden [a]

[a] Institute for Interfacial Catalysis, Pacific Northwest National Laboratory, Richland, WA 99352, USA
[b] Department of Chemistry and Biochemistry, Southern Illinois University, Carbondale, IL 62901, USA

ARTICLE INFO

Article history:
Available online 7 February 2010

Keywords:
Nitrogen oxides
Barium oxide
Alumina
Adsorption
Density functional theory

ABSTRACT

The capability of NO_x storage on the supported BaO catalyst largely depends on the Ba loading. With different Ba loadings, the supported BaO component exposes various phases ranging from well-dispersed nanoclusters to large crystalline particles on the oxide support materials. In order to better understand size and morphological effects on NO_x storage over $\gamma\text{-}Al_2O_3$-supported BaO materials, the adsorption structures and energetics of single NO_2 molecule, as well as $NO_x + NO_y$ ($NO_2 + NO_2$, $NO + NO_3$ and $NO_2 + NO_3$) pairs on the $BaO/\gamma\text{-}Al_2O_3(1\,0\,0)$, $(BaO)_2/\gamma\text{-}Al_2O_3(1\,0\,0)$, and $(BaO)_5/\gamma\text{-}Al_2O_3(1\,0\,0)$ surfaces were investigated using first-principles density functional theory calculations. A single NO_2 molecule prefers to adsorb at basic O_{Ba} site forming anionic nitrate species. Upon adsorption, a charge redistribution in the supported $(BaO)_n$ clusters occurs. Synergistic effects due to the interaction of NO_2 with both the $(BaO)_n$ clusters and the $\gamma\text{-}Al_2O_3(1\,0\,0)$ support enhance the stability of adsorbed NO_2. The interaction between NO_2 and the $(BaO)_n/\gamma\text{-}Al_2O_3(1\,0\,0)$ catalysts was found to be markedly affected by the sizes and morphologies of the supported $(BaO)_n$ clusters. The adsorption energy of NO_2 increases from −0.98 eV on the $BaO/\gamma\text{-}Al_2O_3(1\,0\,0)$ surface to −3.01 eV on $(BaO)_5/\gamma\text{–}Al_2O_3(1\,0\,0)$. NO_2 adsorption on $(BaO)_2$ clusters in a parallel configuration on the $\gamma\text{-}Al_2O_3(1\,0\,0)$ surface is more stable than on dimers oriented in a perpendicular fashion. Similar to the bulk BaO(1 0 0) surface, a supported $(BaO)_n$ cluster-mediated electron transfer induces cooperative effects that dramatically increase the total adsorption energy of $NO_x + NO_y$ pairs on the $(BaO)_n/\gamma\text{-}Al_2O_3(1\,0\,0)$ surfaces. Following the widely accepted NO_2 storage mechanism of $BaO + 3NO_2(g) \rightarrow Ba(NO_3)_2 + NO(g)$, our thermodynamic analysis indicates that the largest energy gain for this overall process of NO_x uptake is obtained on the amorphous monolayer-like $(BaO)_5/\gamma\text{-}Al_2O_3(1\,0\,0)$ surface. This suggests that $\gamma\text{-}Al_2O_3$-supported BaO materials with ~6–12 wt% loadings may provide optimum structures for NO_x storage.

1. Introduction

Alkaline earth oxides (e.g. BaO) supported on γ-alumina (Al_2O_3) have widely been used as storage components in NO_x storage-reduction (NSR) catalysts [1,2]. On the fully formulated catalyst NO_x from the exhaust emission is first oxidized to NO_2 over noble metals (Pt and/or Rh) and then NO_2 is chemisorbed by BaO, forming barium nitrate $Ba(NO_3)_2$ under lean-burn (i.e. oxygen-rich) operating conditions [1,2]. As with most heterogeneous catalytic processes, the reactivity of the NO_x storage, (i.e. the sorption of NO_2 on the BaO component), strongly depends on the chemical and physical nature of the supported active BaO phase. Important questions, like how and where NO_2 interacts with the active sorption sites on supported BaO that may expose different surface structures (morphologies) are yet to be answered. Atomic level understanding of the interaction between NO_2 and alumina-supported BaO with different sizes and structures is essential to improve the effectiveness of current NO_x storage materials.

Without considering other possible Ba-containing compounds such as BaO_2, $Ba(OH)_2$, and $BaCO_3$ that could co-exist and inter-transform with BaO phases under practical cyclic conditions [2–4], sizes and morphologies of the supported BaO phases depend not only on the Ba loading, the preparation method, and the support [5–7], but also on the operating conditions [8]. Using traditional incipient wetness methods with a $Ba(NO_3)_2$ precursor, ultra-high field NMR spectra coupled with ultra-high resolution scanning transmission electron microscopy (HR-STEM) images of the prepared $BaO/\gamma\text{-}Al_2O_3$ storage materials clearly show that well-dispersed nano-sized $(BaO)_x$ ($x \leq 2$) clusters are anchored to penta-coordinated Al^{3+} sites on the $\gamma\text{-}Al_2O_3$ substrate at low Ba (<8 wt%) loadings [9]. At 2 wt% BaO loading, nearly half of the penta-coordinated Al^{3+} sites on the $\gamma\text{-}Al_2O_3(1\,0\,0)$ surface are occupied by

* Corresponding author. Tel.: +1 509 375 6303; fax: +1 509 375 4381.
E-mail address: donghai.mei@pnl.gov (D. Mei).

0920-5861/$ – see front matter © 2010 Elsevier B.V. All rights reserved.
doi:10.1016/j.cattod.2010.01.005

BaO monomers. As the Ba loading increases towards 8 wt%, and then higher-order 2D clusters become the predominant BaO phases. For BaO loadings higher than 20 wt%, both HR-STEM images from high surface area materials and infrared reflection absorption spectroscopy (IRAS) measurement indicate that amorphous 3D BaO clusters are formed on the γ-Al_2O_3 support [9,10].

NO_2 adsorption studies on γ-Al_2O_3-supported BaO with different BaO coverages revealed the formation of two different types of nitrate species [11]. The nomenclature arose because "surface" nitrates were observed to form by NO_2 interacting with supported small BaO clusters or monolayers at low Ba loadings, while the "bulk" nitrates were formed by NO_2 interacting with large, bulk-like BaO particles at high Ba loadings. Important new insights regarding these two nitrate species have recently been provided by comparison of theoretically calculated and experimentally measured vibrational frequencies of both types of nitrate species [9]. In particular, the results showed that "surface" nitrates are those formed on no more than monolayer thick BaO clusters that are themselves anchored to the γ-Al_2O_3(1 0 0) surface. In contrast, "bulk" nitrates are both adsorbed and absorbed NO_x species on bulk-like 3D Ba-containing phase, including adsorbed NO_x on bulk BaO surfaces. Desikusumastuti et al. have described strong size effects on the stability of surface NO_x species formed by the interaction of $NO_2$with nanostructured BaO particles supported on ordered Al_2O_3 films [5]. Using *in situ* IRAS and molecular beam methods, they found that the stability of nitrate species formed on very small BaO particles is much lower than that of bulk-like nitrates formed on large BaO particles, although the rate of nitrate formation over small BaO particles was faster [5]. Due to their low stabilities on the support, the small-particle nitrate species can be rapidly transformed to bulk-like nitrates via an aggregation process. The size dependence of the stability of formed nitrates was explained to be the consequence of the interaction between NO_2 and BaO, which, in turn, was determined by the interaction of supported BaO particles with different sizes as well as the underlying alumina support [5].

The effects of catalyst size and morphology on the NO_2 interaction with BaO have also been theoretically examined [12–22]. The interaction of NO_2 with unsupported BaO clusters, flat and stepped BaO surfaces, and γ-Al_2O_3-supported BaO clusters have been studied using first-principles density functional theory (DFT) calculations [12–22]. Generally, the interaction between NO_2 and BaO can be understood as a combination of Lewis acid–base interactions resulting from strong basicity of BaO and redox (electron transfer) processes [20,23]. In particular, upon adsorption, fractional electron transfer occurs from BaO to the adsorbed NO_2 molecule, forming either anionic nitrite NO_2^- at acidic Ba^{2+} sites or anionic nitrate NO_3^- at Lewis basic O^{2-} sites on BaO. For unsupported BaO clusters, the adsorption energies of NO_2 change with the cluster size. It was found that the adsorption energy of NO_2 in an N-down configuration as NO_3^- species decreased from −1.22 eV on $(BaO)_1$ monomer to −0.86 eV on the $(BaO)_4$ tetramer [16,17], while it increased from −1.07 eV on the $(BaO)_6$ hexamer to −1.28 eV on $(BaO)_{12}$ cluster [22]. Gronbeck et al. explained this moderate size dependence on the basis of the electrostatic nature of the interaction between NO_2 and BaO [22]. Cheng and Ge studied NO_2 adsorption on the edge and corner sites of BaO clusters up to $(BaO)_{32}$, as well as the stepped BaO(3 1 0) surface [17]. They found that the adsorption of NO_2 on the edge and corner sites of the BaO clusters was stronger than on the flat BaO(1 0 0) surface. These authors also investigated the interaction of NO_2 with BaO clusters supported on the Al-terminated γ-Al_2O_3 surface [16,17]. They found a strong synergistic effect that enhances NO_2 adsorption as NO_2 interacts with both BaO clusters and the support. For $NO_x + NO_y$ pair ($x = 1, 2$; $y = 2, 3$) adsorption on the BaO(1 0 0) surface, an enhanced stability has been clearly rationalized by a cooperative co-adsorption mechanism [20,24]. Such increased stability of adsorbed NO_x species on different sizes of unsupported BaO clusters was found to be essentially the same as the $NO_x + NO_y$ pair adsorption on the flat BaO(1 0 0) surface [22].

In order to better understand size and morphological effects on the NO_2 interaction with γ-Al_2O_3-supported BaO, we investigated the adsorption structures and energetics of single NO_2 molecule and $NO_x + NO_y$ pairs on the BaO clusters (BaO monomer, $(BaO)_2$ dimers, and an amorphous $(BaO)_5$ monolayer) supported on the γ-Al_2O_3(1 0 0) surface using first-principles DFT calculations. Three $NO_x + NO_y$ pairs $NO_2 + NO_2$, $NO + NO_3$ and $NO_2 + NO_3$ were chosen to follow generally the accepted consecutive NO_2 storage route over the γ-Al_2O_3-supported BaO materials. The calculation results were then directly compared with our previous results on the clean γ-Al_2O_3(1 0 0) and BaO(1 0 0) surfaces [9,19,25]. Based on a thermodynamic stability analysis, an optimum BaO loading on the γ-Al_2O_3 support for NO_2 storage is proposed.

2. Computational method

Periodic DFT calculations were performed using the Vienna *ab initio* simulation package (VASP) [26,27]. The projector augmented wave (PAW) method combined with a plane-wave basis set and a cutoff energy of 400 eV was used to describe core and valence electrons [28,29]. The Perdew–Burke–Ernzerhof (PBE) form of generalized gradient approximation (GGA) [30] with spin polarization was implemented in all calculations. Ground-state atomic geometries of the entire systems were obtained by minimizing the forces on each atom to below 0.05 eV/Å.

Previous experimental investigations strongly suggest that penta-coordinated Al^{3+} ions are the anchoring sites on the γ-Al_2O_3 support surface for deposited transition metal and metal oxide particles [31,32]. Since the penta-coordinated Al^{3+} sites are only available on the γ-Al_2O_3(1 0 0) surface, a γ-Al_2O_3(1 0 0)-(2 × 1) model surface with eight atomic layers (11.16 Å × 8.41 Å × 8.37 Å) has been used as the support substrate. The γ-Al_2O_3(1 0 0)-(2 × 1) model surface had been thoroughly tested and validated in our previous studies [9,19,25]. The oxide-on-oxide $(BaO)_n$/γ-Al_2O_3(1 0 0) surface models were constructed by structurally optimizing adsorbed $(BaO)_n$ ($n = 1, 2, 5$) clusters on the γ-Al_2O_3(1 0 0) surface [33]. A vacuum slab of 15 Å in the *z*-direction was used to separate the interactions of the neighboring model surface slabs. A (2 × 2 × 1) Monkhorst–Pack mesh sampling scheme was found to be accurate enough for the convergence of adsorption structures and energies after testing different k-point grids ranging from (1 × 1 × 1) to (4 × 4 × 1).

Adsorption energies, E_{ad,NO_2}, of NO_2 on the $(BaO)_n$/γ-Al_2O_3(1 0 0) surfaces were calculated by Eq. (1):

$$E_{ad,NO_2} = E_{NO_2+surface} - (E_{surface} + E_{NO_2}) \quad (1)$$

where $E_{surface}$ is the total energy of the bare $(BaO)_n$/γ-Al_2O_3(1 0 0) surface, E_{NO_2} is the energy of the isolated NO_2 molecule in the vacuum, and $E_{NO_2+surface}$ is the total energy of NO_2 interacting with the $(BaO)_n$/γ-Al_2O_3(1 0 0) surface. Similarly, for $NO_x + NO_y$ pair ($NO_2 + NO_2$, $NO + NO_3$ and $NO_2 + NO_3$) adsorption, the total adsorption energies, E_{ad,NO_x+NO_y}, were calculated as:

$$E_{ad,NO_x+NO_y} = E_{NO_x+NO_y+surface} - (E_{surface} + E_{NO_x} + E_{NO_y}) \quad (2)$$

Based on these definitions, a negative value of E_{ad,NO_2} or E_{ad,NO_x+NO_y} indicates favorable (exothermic) adsorption.

3. Results and discussion

The size and morphology of $(BaO)_n$ clusters supported on the γ-Al_2O_3 surface depend upon the Ba (or BaO) loading and preparation

method [5,9]. Based on HR-STEM images of BaO/γ-Al_2O_3 storage materials with varying BaO coverages, it is clear that monomer $(BaO)_1$ and dimer $(BaO)_2$ clusters are predominant at low coverages, while much larger BaO monolayer clusters and 3D bulk-like particles form at high coverages [9]. We have also computed the morphologies of supported BaO structures obtained by adsorption of varying coverages of BaO monomers interacting with the γ-Al_2O_3(1 0 0) surfaces using DFT [32]. We find that the size and morphology of γ-Al_2O_3-supported $(BaO)_n$ (n = 1–8) clusters via an aggregation process are determined by the BaO coverage. At low BaO coverage, it is thermodynamically unfavorable for isolated BaO monomers to form larger $(BaO)_n$ ($n > 2$) clusters on the dehydrated γ-Al_2O_3(1 0 0) surface by aggregation and the supported $(BaO)_2$ dimer is found to be the most energetically stable cluster size on γ-Al_2O_3 support. However, at high BaO coverages, the formation of a $(BaO)_n$ ($n > 2$) 2D overlayer becomes thermodynamically favorable. In agreement with experimental observations [10], the amorphous monolayer-like $(BaO)_5$ overlayer is formed at BaO coverage of 0.75 ML [32]. As a result, three model oxide-on-oxide surfaces, i.e. BaO/γ-Al_2O_3(1 0 0), $(BaO)_2$/γ-Al_2O_3(1 0 0), and $(BaO)_5$/γ-Al_2O_3(1 0 0) are studied, representing the BaO/γ-Al_2O_3 storage materials at practically different BaO loadings. Although multiple $(BaO)_n$/γ-Al_2O_3(1 0 0) structural configurations with different stabilities were found in our previous work [32], the most stable $(BaO)_n$/γ-Al_2O_3(1 0 0) (n = 1, 2, 5) surface structures shown in Fig. 1 are adopted here as model substrates in this work. For the $(BaO)_2$/γ-Al_2O_3(1 0 0) surface, two types of surface structures with one in the parallel $(BaO)_2$ cluster configuration (Fig. 1b) and another in the perpendicular $(BaO)_2$ cluster configuration (Fig. 1c) are used to examine morphology effects.

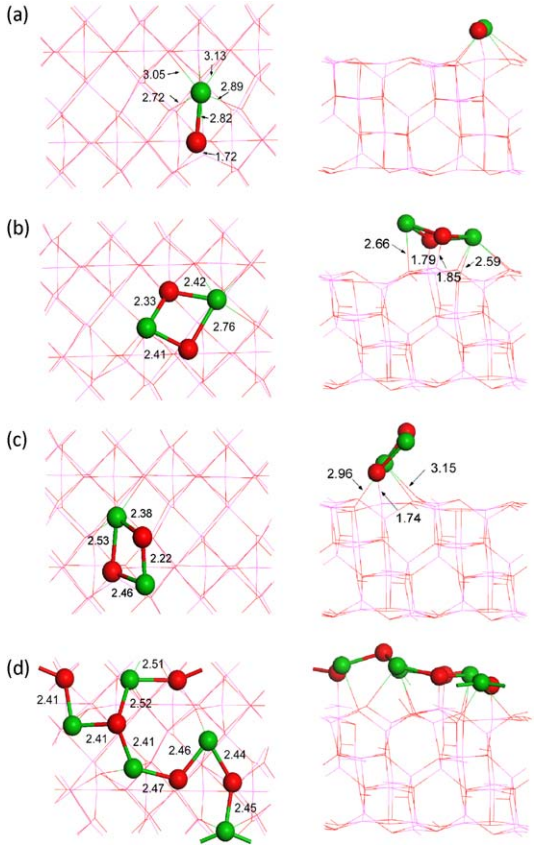

Fig. 1. Optimized structures of various $(BaO)_n$/γ-Al_2O_3(1 0 0) surfaces: (a) BaO/γ-Al_2O_3(1 0 0); (b) $(BaO)_2$/γ-Al_2O_3(1 0 0) in a parallel configuration; (c) $(BaO)_2$/γ-Al_2O_3(1 0 0) in a perpendicular configuration; and (d) $(BaO)_5$/γ-Al_2O_3(1 0 0). Al atoms are in magenta, O atoms in red, and Ba atoms are in green. The bond lengths shown in the figure are in angstrom units. (For interpretation of the references to color in this figure legend, the reader is referred to the web version of the article.)

In the following discussion on the adsorption of NO_2 and $NO_x + NO_y$ pairs on the $(BaO)_n$/γ-Al_2O_3(1 0 0) surfaces, three different types of oxygen atoms are defined: for O_s atom represents the atomic surface oxygen on the γ-Al_2O_3(1 0 0) surface; O_N atoms are the oxygen atom from adsorbed NO_2 (NO or NO_3); and O_{Ba} atoms are the oxygen atom belonging to the BaO clusters (monomer, dimer and pentamer).

3.1. BaO/γ-Al_2O_3 surface

Multiple adsorption configurations have been identified for NO_2 interacting with the BaO monomers on γ-Al_2O_3(1 0 0) as shown in Fig. 2a–c. NO_2 binds solely with the Ba ion in a bidentate structure shown in Fig. 2a. The calculated adsorption energy is −0.44 eV, which is in good agreement with a previous DFT result of −0.41 eV on the spinel γ-Al_2O_3(1 1 1) supported BaO monomer model [16]. The two O_N–Ba bond lengths are almost the same (2.94 and 2.99 Å). Note that the Ba–O_{Ba} bond length is only 2.45 Å after NO_2 adsorption representing a pronounced shortening from the original Ba–O_{Ba} bond length of 2.82 Å (see Fig. 1a), and suggesting a large structural relaxation of the supported BaO monomer occurs upon NO_2 adsorption.

As indicated before, the interaction between NO_x species and the $(BaO)_n$ clusters [16,17,21,22] as well as the BaO(1 0 0) surface [14,15,20] is typically Lewis acid–base one accompanied by significant charge transfer. Indeed, a Bader charge analysis [34,35] performed for this adsorption configuration shows that charge redistribution occurred within the BaO–NO_2 adsorption complex. Upon adsorption, NO_2 becomes $NO_2^{-\delta}$ by obtaining a total 0.47 |e| charge from the supported BaO monomer. Correspondingly, the charge on the Ba atom changes from +1.50 |e| to +1.62 |e| while the charge on the O_{Ba} atom changes from −1.42 |e| to −1.20 |e|. Similar to the adsorption of BaO monomer on the γ-Al_2O_3(1 0 0) surface [32], charge transfer between the γ-Al_2O_3 substrate and the BaO–NO_2 complex is negligible (∼0.05 |e|). This indicates that charge redistribution, induced by NO_2 adsorption, only occurs in the supported BaO monomer, not involving the γ-Al_2O_3 substrate. The contribution of the γ-Al_2O_3 substrate to the adsorption complex is structural rather than electronic. After NO_2 adsorption, the BaO–NO_2 complex, i.e. $(BaO)^{+0.42|e|}(NO_2)^{-0.47|e|}$, is almost neutral.

NO_2 can also adsorb on both Ba and O_{Ba} sites on the BaO/γ-Al_2O_3(1 0 0) surface, in a parallel configuration shown in Fig. 2b. The bond lengths of N–O_{Ba} and Ba–O_N are 2.15 and 2.87 Å, respectively. Similarly, the Ba–O_{Ba} bond length becomes shorter (2.42 Å) after NO_2 adsorption. Bader charge analysis also shows charge redistribution for the BaO–NO_2 complex. NO_2 becomes $(NO_2)^{-0.34|e|}$ as the charge on the Ba ion changes from +1.50 |e| to +1.62 |e|, and the O_{Ba} charge changing from −1.42 |e| to −1.27 |e| after NO_2 adsorption. Again, no noticeable charge transfer between the γ-Al_2O_3 substrate and the BaO–NO_2 complex is found. The adsorption energy of NO_2 in this parallel configuration is −0.56 eV, which is slightly stronger than in the bidentate adsorption structure. This is due to the fact that adsorbed NO_2 can interact with both Ba and O_{Ba} atoms in this parallel configuration.

NO_2 can also adsorb at the interface between the supported BaO monomer and the γ-Al_2O_3(1 0 0) substrate. In this configuration, the adsorbed NO_2 molecule binds with an O_{Ba} ion and a surface Al atom through the N–O_{Ba} and the O_N–Al bonds, forming a nitrate-like NO_3 species. As shown in Fig. 2c, the strong Ba–O_{Ba} bond contraction, induced by NO_2 solely interacting with the supported BaO monomer as described above is slightly abated, the Ba–O_{Ba} bond length being 2.57 Å in this configuration. We note that N–O_{Ba} and N–O_N bonds are

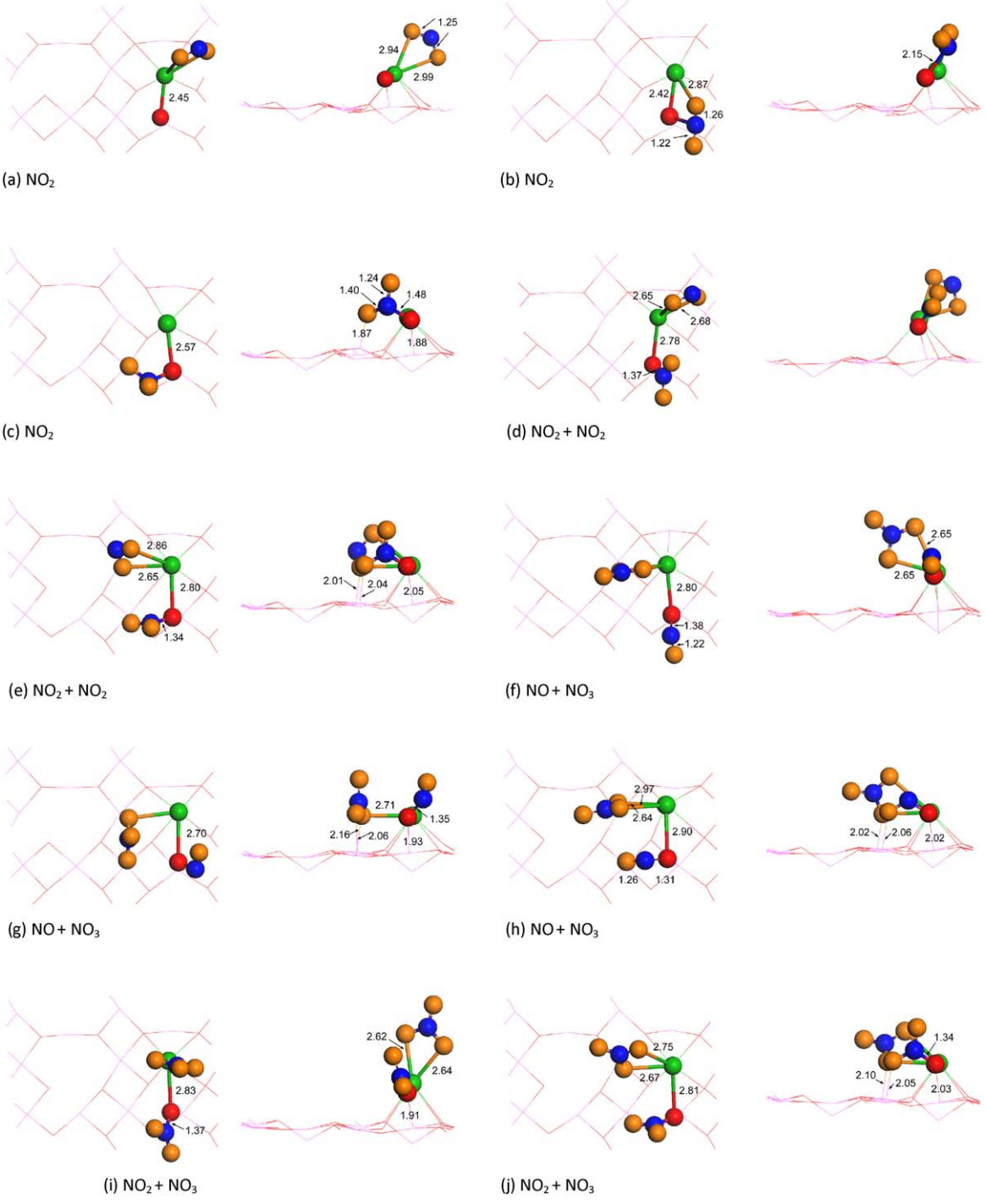

Fig. 2. Adsorption structures of NO_2, as well as NO_2 + NO_2, NO + NO_3 and NO_2 + NO_3 pairs on the BaO/γ–Al_2O_3(1 0 0) surface. For each adsorption structure, both top and side views are shown. The γ-Al_2O_3(1 0 0) substrate is illustrated in faint lines for clarity, and the color scheme of Fig. 1 is applied. The O atoms of adsorbed NO_x (x = 1–3) species are in orange and N atoms are in blue. (For interpretation of the references to color in this figure legend, the reader is referred to the web version of the article.)

elongated to 1.48 and 1.40 Å respectively to accommodate the O_N–Al bond that forms to the γ-Al_2O_3 surface. Both N–O_{Ba} and N–O_N bonds in the thus formed NO_3 are much longer than the calculated N–O bond of 1.25 Å for a NO_3 radical in the gas phase, while the third O–N bond of NO_3 is 1.24 Å. The calculated adsorption energy of NO_2 forming this nitrate-like NO_3 configuration is −0.98 eV, considerably stronger than the other two configurations of NO_2 interacting with the supported BaO monomer. This enhanced stability of NO_2 adsorbing at the interfacial region between the two oxides was also found and described as a synergistic effect in a previous study [16]. Interestingly, except for similar charge redistribution between NO_2 and BaO, our Bader charge analysis shows that the surface O_s atom that directly connects to the bonded surface Al atom, rather than the bonded surface Al atom itself, is oxidized. In particular, the charge of the O_s atom changes from −1.61 |e| to −0.94 |e| as NO_2 adsorbs at the interface. The charges of other surface O_s atoms are still in the normal range of −1.60 to −1.64 |e|. As a result, the electron density of the formed anionic $NO_3^{-\delta}$ (δ = 1.94 |e|) species is donated by both the supported BaO monomer and the Al_2O_3 surface. This is close to the result for $NO_3^{-\delta}$ (δ = 1.79 |e|) bound in a similar configuration with

the spinel γ-Al_2O_3(1 1 1) supported BaO monomer reported by Cheng and Ge [16].

Two different adsorption structures of the NO_2 + NO_2 pair on the BaO/γ-Al_2O_3(1 0 0) surface (Fig. 2d and e) were studied in this work. In the first adsorption structure shown in Fig. 2d, the two NO_2 molecules only interact with the supported BaO monomer with one NO_2 adsorbing at the Ba site and the other at the O_{Ba} site. The calculated adsorption energy for this configuration is −2.34 eV. Compared to single NO_2 adsorption, the stability of NO_2 + NO_2 pair adsorption is dramatically enhanced by 1.34 eV with respect to the combined adsorption energy of ∼−1.00 eV for two single adsorbed NO_2 molecules shown in Fig. 2a and b. This indicates that the cooperative effect that enhances the stability of NO_x pair adsorption on larger alkaline earth oxide clusters as well as flat BaO(1 0 0) surfaces [12–15,20–22,24] is also applicable to the γ-Al_2O_3-supported BaO monomers. The enhanced stability is reflected by structural variations upon the pair adsorption. Firstly, the Ba–O_{Ba} bond length becomes 2.78 Å after the NO_2 + NO_2 pair adsorption, which is very close to the original Ba–O_{Ba} bond length (2.82 Å) of the supported, adsorbate-free BaO monomer. The strong Ba–O_{Ba} bond contraction calculated for single NO_2 adsorption is largely eliminated by the second NO_2 adsorption. Secondly, by comparison of Fig. 2a and d, two O_N–Ba bonds for the adsorbed NO_2 on the Ba site are shorter (2.65 and 2.68 Å) in the NO_2 + NO_2 pair adsorption. Also, the N–O_{Ba} bond in the pair adsorption structure is shorter than that for single NO_2 adsorption on the O_{Ba} site. This suggests that, on one hand, the interaction between the supported BaO monomer and the γ-Al_2O_3(1 0 0) substrate becomes weaker, and, on the other hand, the interaction between the supported BaO monomer and NO_2 becomes stronger upon the second NO_2 adsorption. As a consequence, the interaction between NO_2 and the supported BaO monomer, in terms of the total adsorption energy, is dramatically increased. Bader charge analysis shows that both adsorbed NO_2 molecules are oxidized to anionic $NO_2^{-\delta}$ species after adsorption. One of the adsorbed NO_2 actually forms the $NO_2^{-\delta}$ (δ = 1.26 |e|) species by combining with the O_{Ba} atom. In the second NO_2 + NO_2 pair adsorption configuration studied here, both adsorbed NO_2 molecules not only interact with the BaO monomer, but also the γ-Al_2O_3(1 0 0) substrate. Similar to the binding of single NO_2 molecule bound at the BaO–γ-Al_2O_3 interface, a synergistic effect further enhances the stability of adsorbed NO_2 + NO_2 pair in this configuration. The calculated adsorption energy is −3.05 eV, which is 0.75 eV stronger than the adsorption configuration where only the supported BaO monomer is involved.

The NO + NO_3 pairs on γ-Al_2O_3-supported BaO catalysts have been considered as an important intermediate state leading to the formation of $Ba(NO_3)_2$ [11,36]. As such, three different adsorption structures of NO + NO_3 pair on the BaO/γ-Al_2O_3(1 0 0) surface were studied. In the first structure shown in Fig. 2f, both NO and NO_3 interact only with the supported BaO monomer. NO binds with the O_{Ba} site and NO_3 adsorbs at the Ba site in a bidentate structure. Bader charge analysis shows that the adsorbed NO in this pair adsorption structure is positively charged (+0.26 |e|). As such, the adsorbed NO + NO_3 pair can be described as the $NO^{+\chi}NO_3^{-\delta}$ pair. However, adsorbed NO is not positively charged in the other two co-adsorbed structures (Fig. 2g and h) when the γ-Al_2O_3 substrate is directly involved in the adsorption. For these latter two adsorption configurations of the NO + NO_3 pair, fractional electron charge (0.44 and 0.11 |e|) was found to be transferred from the γ-Al_2O_3 substrate to the $NO^{+\chi}NO_3^{-\delta}$ pair upon adsorption. Once again, the calculated adsorption energies of the NO + NO_3 pair in these three different structures confirm a synergistic effect that enhances stability. The adsorption energy of the NO + NO_3 pair gradually increases from −3.67 eV for the structure where the NO + NO_3 pair exclusively interacts with the supported BaO monomer (Fig. 2f), to −4.07 eV for the structure in which NO_3 interacts with both the BaO monomer and the γ-Al_2O_3 substrate (Fig. 2g), and further to −4.19 eV for the structure where both NO and NO_3 bind with the BaO monomer and the γ-Al_2O_3 substrate (Fig. 2h).

For the adsorption of the NO_2 + NO_3 pairs on the BaO/γ-Al_2O_3(1 0 0) surface, stoichiometric $Ba(NO_3)_2$ species are formed on the γ-Al_2O_3 substrate. Here we only present two typical adsorption structures. The first structure, shown in Fig. 2i, is the NO_2 + NO_3 pair adsorbed on the supported BaO monomer without interacting with the support while the second structure (Fig. 2j) involves NO_x interacting with both BaO monomer and the γ-Al_2O_3 substrate. Again the second structure is 0.36 eV stronger than the first structure due to the synergistic effect. These two structures have been identified as the basis for "surface" nitrates formed on BaO/γ-Al_2O_3 catalysts using a combined experimental and theoretical method [9].

The calculated adsorption energies and Bader charges of NO_2 and the NO_x + NO_y pairs on BaO/γ-Al_2O_3(1 0 0) surface are summarized in Tables 1 and 2. We would point out that the adsorption structures of NO_2 and the NO_x + NO_y pairs on BaO/γ-Al_2O_3(1 0 0) surface that lack of direct interactions with the γ-Al_2O_3(1 0 0) surface are spatially flexible. For each adsorption configuration reported here, we have identified several structures with different molecular orientations (not shown here). The adsorption energy difference between these adsorption structures is less than 0.15 eV.

3.2. $(BaO)_2$/γ-Al_2O_3 surfaces

Our previous calculation showed that two types of structures (parallel and perpendicular) for supported $(BaO)_2$ clusters on the

Table 1
Adsorption energies and Bader charges (in |e|) of NO_2 on $(BaO)_n$/γ-Al_2O_3(1 0 0) (n = 1, 2, 5) surfaces.

Structure	E_{ad} (eV)	Bader charge |e|				
		Ba	O_{Ba}	NO_2	O_s	BaO
BaO/γ-Al_2O_3(1 0 0)		+1.50	−1.42		−1.62	
Fig. 2a	−0.44	+1.62	−1.20	−0.47		+0.42
Fig. 2b	−0.56	+1.62	−1.27	−0.34		+0.35
Fig. 2c	−0.98	+1.63	−0.56	−0.87	−0.94*	+1.07
$(BaO)_2$/γ-Al_2O_3(1 0 0)		+1.50	−1.43		−1.62	
Fig. 3a	−1.17	+1.60	−1.18	−0.79		+0.42
Fig. 3b	−1.53	+1.59	−1.11; −0.80*	−0.89		+0.48
Fig. 4a	−0.97	+1.59	−1.19	−0.87		+0.40
Fig. 4b	−0.45	+1.60	−0.97; −0.57*	−0.83		+0.63
$(BaO)_5$/γ-Al_2O_3(1 0 0)		+1.49	−1.47		−1.62	+0.02
Fig. 5a	−1.64	+1.54	−1.35	−0.88		+0.19
Fig. 5b	−3.01	+1.52	−1.34; −0.82*	−0.86		+0.18

Note: The number with the star "*" is the Bader charge of the bonded O_{Ba} atom.

Table 2
Adsorption energies and Bader charges (in |e|) of $NO_x + NO_y$ ($x = 1–2$, $y = 2–3$) pairs on $(BaO)_n/\gamma\text{-}Al_2O_3(1\,0\,0)$ ($n = 1, 2, 5$) surfaces.

Substrate	Structure	E_{ad} (eV)	Bader charge |e|						
	$NO_2 + NO_2$		Ba	O_{Ba}	NO	NO_2	NO_3	$NO + O_{Ba}$	$NO_2 + O_{Ba}$
$BaO/\gamma\text{-}Al_2O_3(1\,0\,0)$	Fig. 2d	−2.34	+1.65	−0.79		−0.52; −0.40			−1.26
$BaO/\gamma\text{-}Al_2O_3(1\,0\,0)$	Fig. 2e	−3.05	+1.64	−0.81		−0.42; −0.28			−1.11
$(BaO)_2/\gamma\text{-}Al_2O_3(1\,0\,0)$	Fig. 3c	−3.64							
$(BaO)_2/\gamma\text{-}Al_2O_3(1\,0\,0)$	Fig. 4c	−4.44	+1.62	−1.47; −0.67*		−0.84; −0.22			−1.02
$(BaO)_2/\gamma\text{-}Al_2O_3(1\,0\,0)$	Fig. 4d	−4.37							
$(BaO)_5/\gamma\text{-}Al_2O_3(1\,0\,0)$	Fig. 5c	−6.54	+1.56	−1.28; −0.62*		−0.84; −0.35			−0.99
$(BaO)_5/\gamma\text{-}Al_2O_3(1\,0\,0)$	Fig. 5d	−6.21	+1.55	−1.29; −0.59*		−0.89; −0.33			−1.03
Substrate	Structure	E_{ad} (eV)	Bader charge |e|						
	$NO + NO_3$		Ba	O_{Ba}	NO	NO_2	NO_3	$NO + O_{Ba}$	$NO_2 + O_{Ba}$
$BaO/\gamma\text{-}Al_2O_3(1\,0\,0)$	Fig. 2f	−3.67	+1.66	−0.90	+0.26		−1.07	−0.50	
$BaO/\gamma\text{-}Al_2O_3(1\,0\,0)$	Fig. 2g	−4.07	+1.65	−0.83	−0.34		−0.90	−1.16	
$BaO/\gamma\text{-}Al_2O_3(1\,0\,0)$	Fig. 2h	−4.19	+1.67	−0.78	−0.12		−0.88	−1.01	
$(BaO)_2/\gamma\text{-}Al_2O_3(1\,0\,0)$	Fig. 3d	−4.52	+1.59	−0.73	−0.05		−0.89	−0.89	−0.91
$(BaO)_5/\gamma\text{-}Al_2O_3(1\,0\,0)$	Fig. 5e	−7.69	+1.55	−1.30; −0.67*	−0.22		−0.92	−0.89	−0.92
Substrate	Structure	E_{ad} (eV)	Bader charge |e|						
	$NO_2 + NO_3$		Ba	O_{Ba}	NO	NO_2	NO_3	$NO + O_{Ba}$	$NO_2 + O_{Ba}$
$BaO/\gamma\text{-}Al_2O_3(1\,0\,0)$	Fig. 2i	−3.67	+1.67	−0.84		−0.05	−0.84		−0.87
$BaO/\gamma\text{-}Al_2O_3(1\,0\,0)$	Fig. 2j	−4.13	+1.67	−0.76		+0.03	−1.05		−0.88
$(BaO)_2/\gamma\text{-}Al_2O_3(1\,0\,0)$	Fig. 3e	−4.76							
$(BaO)_2/\gamma\text{-}Al_2O_3(1\,0\,0)$	Fig. 3f	−6.07							
$(BaO)_5/\gamma\text{-}Al_2O_3(1\,0\,0)$	Fig. 5f	−5.53							

Note: The number with the star "*" is the Bader charge of the bonded O_{Ba} atom.

$\gamma\text{-}Al_2O_3(1\,0\,0)$ surface are stable, with the parallel configuration is energetically more stable than the perpendicular configuration [32]. For the parallel configuration shown in Fig. 1b, all Ba and O atoms of the $(BaO)_2$ dimer bind with the $\gamma\text{-}Al_2O_3(1\,0\,0)$ surface via Ba–O_s and O_{Ba}–Al bonds. For the perpendicular configuration shown in Fig. 1c, only one BaO unit of the dimer pair binds with the $\gamma\text{-}Al_2O_3(1\,0\,0)$ surface. We first investigated the adsorption of NO_2 on the parallel $(BaO)_2/\gamma\text{-}Al_2O_3(1\,0\,0)$ surface. Fig. 3a and b shows two stable adsorption structures of NO_2 interacting only with the supported $(BaO)_2$ dimer. The adsorption of NO_2 at the O_{Ba} site

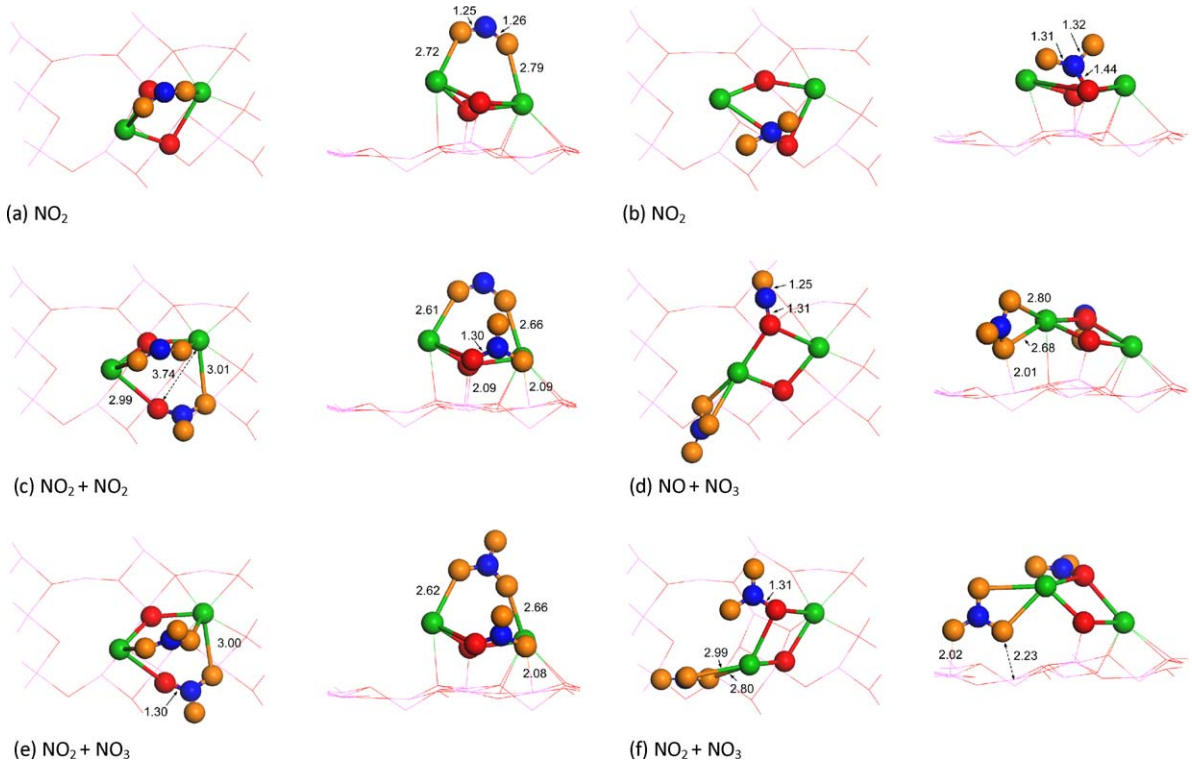

Fig. 3. Adsorption of NO_2, as well as $NO_2 + NO_2$, $NO + NO_3$ and $NO_2 + NO_3$ pairs on the parallel $(BaO)_2/\gamma\text{–}Al_2O_3(1\,0\,0)$ surface. For each adsorption structure, both top and side views are shown, and the color scheme of Fig. 2 is applied.

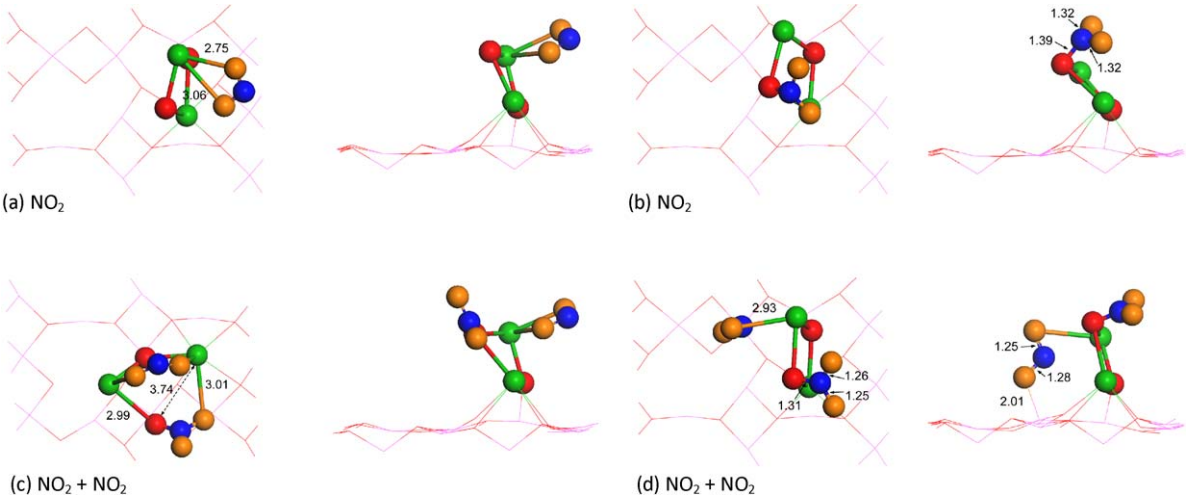

Fig. 4. Adsorption of NO_2 and pairs on the perpendicular $(BaO)_2/\gamma$–Al_2O_3(1 0 0) surface. For each adsorption structure, both top and side views are shown, and the color scheme of Fig. 2 is applied.

through an N–O_{Ba} bond (Fig. 3a, −1.53 eV) is stronger than binding at the Ba sites in a bridging bidentate configuration (Fig. 3b, −1.17 eV). Compared to similar adsorption structures of NO_2 on the BaO/γ-Al_2O_3(1 0 0) surface, the stabilities of NO_2 on the parallel $(BaO)_2/\gamma$-Al_2O_3(1 0 0) surface are significantly increased, indicating that increasing the size of the supported BaO clusters increases the stability of NO_2 adsorption. As found for the monomeric BaO structure, charge redistribution between the supported $(BaO)_2$ dimer and NO_2 occurs upon adsorption. Fractional electronic charge from both O_{Ba} atoms is transferred to the adsorbed NO_2 forming $NO_2^{-0.79|e|}$ and $NO_2^{-0.89|e|}$ in the bridging bidentate structure and the N-down structure, respectively. For the N-down binding structure (Fig. 3b), the charge of the bonding O_{Ba} atom is reduced to −0.80 |e|. Electron transfer between the supported $(BaO)_2$ dimer and the γ-Al_2O_3(1 0 0) substrate is less than 0.1 |e|.

We then studied the adsorption of $NO_x + NO_y$ pairs on the parallel $(BaO)_2/\gamma$-Al_2O_3(1 0 0) surface. The adsorption of NO_2 + -NO_2 pair causes pronounced structural relaxation of the $(BaO)_2$ dimer. As shown in Fig. 3c, although one adsorbed NO_2 molecule locates above the $(BaO)_2$ dimer, the strong interaction between the second adsorbed NO_2 and the $(BaO)_2$ dimer via the N–O_{Ba} bonding causes the adsorbed NO_2 molecule to tilt towards the γ-Al_2O_3(1 0 0) surface. As a result, the adsorbed NO_2 in the N-down configuration binds with both $(BaO)_2$ units of the dimer, as well as with the γ-Al_2O_3(1 0 0) surface. In addition, one of Ba–O_{Ba} bonds in the supported $(BaO)_2$ cluster is broken as a result of the $NO_2 + NO_2$ pair adsorption. The adsorption energy of this $NO_2 + NO_2$ pair adsorption configuration on the $(BaO)_2/\gamma$-Al_2O_3(1 0 0) surface is −3.64 eV. This value is larger than the corresponding adsorption energy on the BaO/γ-Al_2O_3(1 0 0) surface, again implying that the adsorption stabilities of single NO_2 molecule as well as $NO_2 + NO_2$ pairs increase with the size of the supported BaO clusters. The adsorption of NO + NO_3 pairs on the parallel $(BaO)_2/\gamma$-Al_2O_3(1 0 0) surface is shown in Fig. 3d. Although the supported $(BaO)_2$ cluster is still intact in this adsorption configuration, one of the O_{Ba} atoms moves away from the γ-Al_2O_3(1 0 0) surface and, in fact, this O_{Ba}–Al bond is broken.

Structural relaxations induced by $NO_2 + NO_3$ pair adsorption on the $(BaO)_2/\gamma$-Al_2O_3(1 0 0) surface are also found. In the case shown in Fig. 3e, one of the Ba–O bonds in the supported $(BaO)_2$ dimer is broken as a result of the NO_x pair adsorption. Even more profound structural changes are shown in Fig. 3f where the supported $(BaO)_2$ dimer changes its configuration due to the $NO_2 + NO_3$ pair adsorption. In this case, the adsorbed $(BaO)_2$ dimer with initial parallel configuration on the γ-Al_2O_3(1 0 0) surface is now oriented in the perpendicular configuration. As indicated before, the supported $(BaO)_2$ dimer in the perpendicular configuration is less stable than the parallel configuration. Thus, the $NO_2 + NO_3$ pair adsorption leads to a significant weakening of the interaction between the formed $Ba(NO_3)_2$ and the γ-Al_2O_3(1 0 0) surface, likely promoting the mobility of the $Ba(NO_3)_2$. Such a result is consistent with previous experimental observations. In particular, Desikusumastuti et al. [5] observed that surface nitrate species can be readily formed on very small alumina-supported BaO particles. These surface nitrate species can be rapidly transformed to bulk-like nitrates via aggregation processes due to their low stability. Comparing the adsorption energies of the two structures following $NO_2 + NO_3$ pair adsorption shown in Fig. 3e and f, we find that the adsorption of $NO_2 + NO_3$ pairs with the intact $(BaO)_2$ cluster (3f, −6.07 eV) is much stable than the $NO_2 + NO_3$ pair with the broken $(BaO)_2$ cluster (−4. 76 eV).

To further investigate morphology effects on the interaction between NO_x and supported BaO clusters on the γ-Al_2O_3 surface, we investigated the adsorptions of NO_2 and the $NO_2 + NO_2$ pair on the perpendicular $(BaO)_2/\gamma$-Al_2O_3(1 0 0) surface, with the optimized adsorption structures shown in Fig. 4. The corresponding adsorption energies are also given in Tables 1 and 2. For this initial supported dimer morphology, different trends for single NO_2 and $NO_2 + NO_2$ pair adsorption are found. Compared to the parallel $(BaO)_2/\gamma$-Al_2O_3(1 0 0) surface, our calculations show that the adsorption of NO_2 is considerably weaker, while the $NO_2 + NO_2$ pair adsorption is, in fact, somewhat stronger on the perpendicular $(BaO)_2/\gamma$-Al_2O_3(1 0 0) surface.

3.3. Amorphous BaO overlayer supported on γ-Al_2O_3

The DFT-optimized amorphous monolayer-like $(BaO)_5/\gamma$-Al_2O_3(1 0 0) surface is shown in Fig. 1d. A variety of possible adsorption sites on the supported $(BaO)_5$ overlayer are available. In this work, two adsorption sites, NO_2 adsorbing at one of the surface Ba or the O_{Ba} sites, are considered. Fig. 5a shows NO_2 adsorbed at a Ba site in a bidentate structure forming anionic $NO_2^{-\delta}$ (δ = 0.88 |e|) species. Bader charge analysis indicates that no localized electron hole is found at the O_{Ba} sites in the amorphous $(BaO)_5$ overlayer. As given in Table 1, the average charge of Ba atoms increases from +1.49 to +1.54 |e| while the average charge of O_{Ba} atoms decreases from −1.47 to −1.35 |e| after NO_2 adsorption. As a result, the $(BaO)_5$ overlayer is slightly positively charged (+0.19 |e|). For NO_2 adsorption at the O_{Ba} site shown in Fig. 5b, although a similar

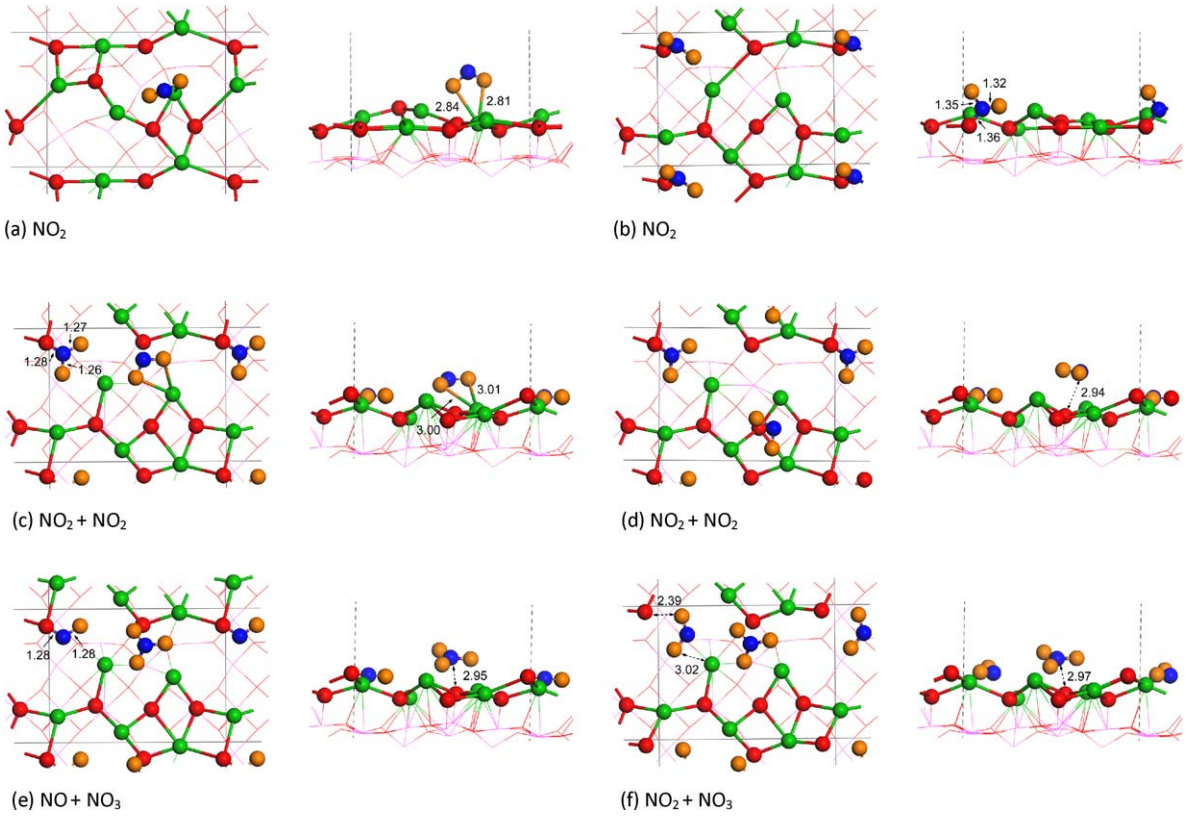

Fig. 5. Adsorption of NO_2, as well as $NO_2 + NO_2$, $NO + NO_3$ and $NO_2 + NO_3$ pairs on the $(BaO)_5/\gamma\text{-}Al_2O_3(1\,0\,0)$ surface. For each adsorption structure, both top and side views are shown, and the color scheme of Fig. 2 is applied.

positively charged (+0.18 |e|) $(BaO)_5$ overlayer is formed, an electron hole located at the bonded O_{Ba} atom is identified. The Bader charge of this O_{Ba} atom is −0.82 |e|, which is clearly different from other O_{Ba} atoms in the $(BaO)_5$ overlayer. The adsorbed NO_2 combining with this reduced O_{Ba} atom can be considered as a $NO_3^{-\delta}$ nitrate species with a total charge of −1.38 |e|. The calculated adsorption energies of NO_2 at the Ba and the O_{Ba} sites are −1.64 and −3.01 eV respectively; obviously, the adsorption of NO_2 at the O_{Ba} site is much stronger than the adsorption at the Ba site. This is consistent with the trend that NO_2 adsorption at O_{Ba} sites on both $BaO/\gamma\text{-}Al_2O_3(1\,0\,0)$ and $(BaO)_2/\gamma\text{-}Al_2O_3(1\,0\,0)$ surfaces is stronger. The adsorption strength of single NO_2 also clearly increases with the BaO cluster size (see Table 1). Furthermore, the effect of the alumina support can be elucidated by comparing the adsorption of NO_2 on the supported amorphous $(BaO)_5$ overlayer with the BaO(1 0 0) surface. The calculated adsorption energy of NO_2 in the most stable structure on the flat BaO(1 0 0) surface is −0.96 eV, which is much weaker than the energies of −1.64 and −3.01 eV on the $(BaO)_5/\gamma\text{-}Al_2O_3(1\,0\,0)$ surface. The enhanced stability of NO_2 on the $(BaO)_5/\gamma\text{-}Al_2O_3(1\,0\,0)$ surface can be attributed to the low-coordination of the adsorption sites compared to the sites on the flat surface [17,21]. This is consistent with the DFT results of NO_2 adsorption on variously coordinated Ba and O sites on unsupported clusters and stepped BaO surfaces [13,17,21]. For instance, Branda et al. found the adsorption energy of NO_2 at the step and corner sites of Ba_9O_9 clusters was about −1.8 eV, almost twice as much as the adsorption energy on the terrace sites (−0.94 eV) [21]. Cheng and Ge also found that the adsorption energies of NO_2 at the step-edge and terrace sites on a stepped BaO(3 1 0) surface were −1.13 and −1.39 eV [17], stronger than on the flat BaO(1 0 0) surface.

For $NO_2 + NO_2$ pair adsorption on the $(BaO)_5/\gamma\text{-}Al_2O_3(1\,0\,0)$ surface, two co-adsorption structures were studied. The calculated adsorption energies are −6.54 and −6.21 eV, respectively, indicating a significant enhancement of stability upon the second NO_2 adsorption. As shown in Fig. 5c and d, one NO_2 molecule binds with the O_{Ba} sites forming anionic $NO_3^{-\delta}$ with a very similar structure to a single NO_2 adsorption on the O_{Ba} site shown in Fig. 5b. The second NO_2 adsorbs on either the Ba site in a bidentate configuration (Fig. 5c) or over the O_{Ba} site in the parallel configuration forming $NO_2^{-\delta}$ (Fig. 5d). Compared to the single NO_2 adsorption, more electrons are transferred from the $(BaO)_5$ overlayer to the adsorbed $NO_2 + NO_2$ pair. For the $NO + NO_3$ and $NO_2 + NO_3$ pairs, the optimized adsorption structures are shown in Fig. 5e and f, with calculated adsorption energies of −7.69 eV for the $NO + NO_3$ pair and −5.53 eV for the $NO_2 + NO_3$ pair. Interestingly, we observe that NO_3 adsorbs on the $(BaO)_5/\gamma\text{-}Al_2O_3(1\,0\,0)$ surface in a parallel fashion for both adsorption structures. This parallel adsorbed NO_3 structure is not found for the $NO_x + NO_3$ pairs on the $BaO/\gamma\text{-}Al_2O_3(1\,0\,0)$ and $(BaO)_2/\gamma\text{-}Al_2O_3(1\,0\,0)$ surfaces, but has been calculated to be the most stable adsorption configuration on the flat BaO(1 0 0) surface in previous theoretical studies [9,19,25]. This indicates that the nature of $(BaO)_5/\gamma\text{-}Al_2O_3(1\,0\,0)$ surface more closely resembles the extended BaO(1 0 0) surface rather than the $\gamma\text{-}Al_2O_3(1\,0\,0)$-supported BaO monomers and $(BaO)_2$ dimers.

3.4. Effects of Ba loading on NO_x storage

The NO_x storage capability over the $\gamma\text{-}Al_2O_3$-supported BaO materials depends not only on the BaO loading, but also on the morphology of BaO particles on the support. Previous experimental and theoretical studies [5,9,10,32,33] clearly indicate that nano-sized BaO clusters such as BaO monomers and $(BaO)_2$ dimers are the primary BaO phases present on the support at very low Ba loadings (<4 wt%). At low to intermediate Ba loadings

Table 3
Reaction energies ΔE (eV) of various elementary steps of NO_x storage on different model surfaces.

Reaction	γ-Al_2O_3 (1 0 0)	BaO/γ-Al_2O_3 (1 0 0)	$(BaO)_2$/γ-Al_2O_3 (1 0 0)	$(BaO)_5$/γ-Al_2O_3 (1 0 0)	BaO (1 0 0)
Substrate + $3NO_2$(g) = substrate + NO_2^- + $2NO_2$(g)	−0.22	−0.96	−1.53	−3.01	−0.96
Substrate + NO_2^- + $2NO_2$(g) = substrate + NO_2^- + NO_2^- + NO_2(g)	+0.04	−2.68	−2.11	−3.59	−1.75
Substrate + NO_2^- + NO_2^- + NO_2(g) = substrate + NO^- + NO_3^- + NO_2(g)	−0.53	+0.57	+0.20	+0.02	−0.30
Substrate + NO^- + NO_3^- + NO_2(g) = substrate + NO_2^- + NO_3^- + NO(g)	+0.48	+0.06	−0.27	+2.17	−0.02
Substrate + $3NO_2$(g) = substrate + NO_2^- + NO_3^- + NO(g)	−0.27	−3.01	−3.68	−4.41	−3.13

(∼6–12 wt%), amorphous 2D BaO clusters are formed. At still higher Ba loadings (>15 wt%), bulk-like BaO particles become the dominant BaO phase on the γ-Al_2O_3 substrate. Therefore, both the size and the morphology of the BaO phase on the alumina support vary with Ba loading. In this work, the BaO/γ-Al_2O_3(1 0 0) and $(BaO)_2$/γ-Al_2O_3(1 0 0) substrates are useful models for representing the γ-Al_2O_3-supported BaO materials at low (≤4 wt%) Ba loadings, and the $(BaO)_5$/γ-Al_2O_3(1 0 0) system can be used for modeling supported BaO materials at intermediate BaO loading (∼6–12 wt%). We previously investigated the adsorption of NO_2 and NO_x + NO_y pairs on the clean γ-Al_2O_3(1 0 0) surface and the "bulk" BaO(1 0 0) surface [9,19,25] which are representative of the BaO-free support and the γ-Al_2O_3-supported BaO materials with very high Ba loadings. With the new results presented here, we can now compare the NO_x storage capability of γ-Al_2O_3-supported BaO materials for a full range of Ba loadings.

Despite extensive experimental and theoretical studies carried out in the past 10 years (see review papers [1,2] and references therein), details of the complex NO_x storage mechanism for γ-Al_2O_3-supported BaO materials remain unclear. However, a notable generally agreed-upon aspect of this mechanism, based on experimental work, is the operation of stoichiometric storage [37–39], given in Eq. (3):

$$BaO + 3NO_2(g) = Ba(NO_3)_2 + NO(g) \quad (3)$$

According to this mechanism, NO_2 is the primary form of NO_x being sorbed by the BaO phase. For every three NO_2 molecules that react with the BaO phase, stoichiometric barium nitrate $Ba(NO_3)_2$ will be formed along with the release of one NO molecule into the gas phase. This mechanism for NO_x storage has been widely used in previous DFT studies of NO_x storage on BaO(1 0 0) surfaces [12–15,20,22], and is also considered here to compare the relative storage behavior as a function of BaO loading on the γ-Al_2O_3(1 0 0) surface. For these various model catalysts, the reaction energies of possible elementary steps involving each of the three NO_2 adsorption and reaction processes are given in Table 3. The adsorption energies of single NO_2, as well as NO_2 + NO_2, NO + NO_3 and NO_2 + NO_3 pairs in their most stable configurations were used to calculate the reaction energies. In this comparison, the total energy gain was referenced to the clean substrate and three NO_2 molecules in the gas phase.

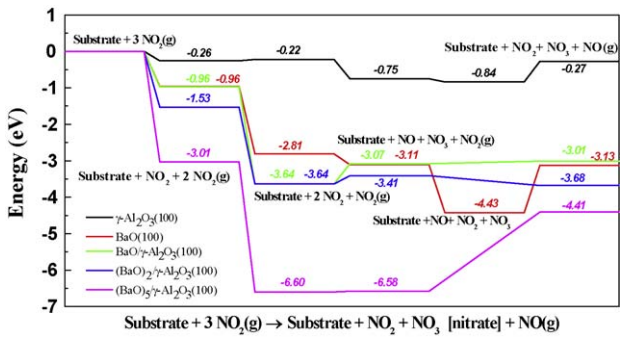

Fig. 6. Thermodynamical energy diagram of NO_2 storage on different substrates.

As shown in Fig. 6, the energy profile for NO_2 storage on the clean γ-Al_2O_3(1 0 0) surface is rather flat. In the absence of Ba, the γ-Al_2O_3 surface only weakly interacts with NO_2 and NO_x + NO_y pairs. This is consistent with experiments that the γ-Al_2O_3 support itself plays a minor role in NO_x storage. On the γ-Al_2O_3-supported BaO monomer surface, a strong interaction between NO_2 and the substrate is present. The synergistic effect for NO_2 interacting with both BaO monomer and the γ-Al_2O_3 support leads to NO_2 adsorption that is as strong as on the BaO(1 0 0) surface. We noted above that the cooperative effect of NO_x + NO_y pair adsorption is more pronounced on the supported BaO monomer than the flat BaO(1 0 0) surface, as evidenced by the adsorption energy for NO_2 + NO_2 pairs of −3.64 eV on BaO/γ-Al_2O_3(1 0 0), which is 0.83 eV stronger than on the BaO(1 0 0) surface. A further interconversion from the NO_2 + NO_2 pairs to adsorbed NO + NO_3 pairs on the supported BaO monomer and the flat BaO(1 0 0) surface proceeds with different energetic, being endothermic on the supported BaO monomer while it is exothermic on the BaO(1 0 0) surface. As a result, nearly identical adsorption strengths are obtained for NO + NO_3 pairs on both surfaces. For the formation of the final stoichiometric product of $Ba(NO_3)_2$ (modeled as a co-adsorbed NO_2 + NO_3 pair with adsorbed NO_2 bound to a surface O species), the total energy gain for the γ-Al_2O_3-supported BaO monomer and the BaO(1 0 0) surface is −3.01 and −3.13 eV, respectively. Our previous experimental and theoretical studies have suggested that supported $(BaO)_2$ clusters are the most thermodynamically favorable BaO phase on the γ-Al_2O_3 support at low Ba loadings [9,33]. The results presented here (Fig. 6) also show that the thermodynamics of NO_x uptake via this reaction mechanism is very similar for both the supported BaO monomers and $(BaO)_2$ dimers. At intermediate Ba loadings, however, NO_2 interactions are dramatically enhanced by the size and amorphous structure of the supported $(BaO)_5$ overlayer. The adsorption strengths of NO_2 and NO_x + NO_y pairs on the $(BaO)_5$/γ-Al_2O_3(1 0 0) surface are almost twice those on the $(BaO)_2$/γ-Al_2O_3(1 0 0) surface. In addition, the energy gain for the entire storage process on the $(BaO)_5$/γ-Al_2O_3(1 0 0) surface is 0.73 and 1.23 eV higher than the supported $(BaO)_2$/γ-Al_2O_3(1 0 0) and BaO(1 0 0) surfaces. This result suggests that BaO structures present at intermediate Ba loadings, ranging from 6 to 12 wt%, a coverage range where "surface" nitrates have been observed as the primary form of stored NO_x, provide an optimum Ba morphology for NO_x uptake in γ-Al_2O_3-supported BaO materials.

4. Conclusions

NO_x storage over γ-Al_2O_3-supported BaO materials were investigated using first-principles DFT calculations. Three model substrates were used to represent the γ-Al_2O_3-supported BaO materials at different Ba loadings: the γ-Al_2O_3-supported BaO monomer and $(BaO)_2$ dimer surfaces for low Ba loadings and the γ-Al_2O_3-supported amorphous monolayer-like $(BaO)_5$/γ-Al_2O_3(1 0 0) surface for the intermediate Ba loadings. The adsorption structures and energetics of single NO_2 molecules and NO_x + NO_y (NO_2 + NO_2,

NO + NO_3 and NO_2 + NO_3) pairs on these three $(BaO)_n/\gamma$-Al_2O_3(1 0 0) (n = 1, 2, 5) surfaces were investigated. The adsorption of NO_2 on the $(BaO)_n/\gamma$-Al_2O_3(1 0 0) surfaces can be described as an acid–base interaction with electron transfer due to the strong basic nature of BaO. NO_2 preferentially adsorbs at oxygen sites of the supported BaO forming anionic nitrate-like species while $NO_x + NO_y$ pairs favor adsorption at Ba and O sites forming nitrite and/or nitrate species, consistent with prior experimental observations. For single NO_2 molecule adsorption, a pronounced synergistic effect was found on the BaO/γ-Al_2O_3(1 0 0) and $(BaO)_2/\gamma$-Al_2O_3(1 0 0) surfaces resulting from interactions with both the nano-sized BaO clusters and the γ-Al_2O_3 support. With increasing BaO cluster size, the adsorption strength of NO_2 increases. Furthermore, the interaction of NO_2 with BaO is affected by morphology as evidenced by the result that adsorption of both NO_2 and $NO_x + NO_y$ pairs on the supported parallel $(BaO)_2$ clusters are stronger than on supported perpendicular $(BaO)_2$ clusters. Similar to $NO_x + NO_y$ pair adsorption on BaO(1 0 0), cooperative effects that dramatically enhance the stability of the adsorbed NO_x are also found for NO_x adsorption on the γ-Al_2O_3-supported $(BaO)_n$ systems. Most significantly, by comparing the new results presented here with the adsorption energies of BaO-free γ-Al_2O_3(1 0 0) and flat BaO(1 0 0) surfaces, we find that the largest energy gain for an overall storage process that leads to stoichiometric $Ba(NO_3)_2$ and gas phase NO is obtained on the amorphous, monolayer-like $(BaO)_5/\gamma$-Al_2O_3(1 0 0) surface. This indicates that the γ-Al_2O_3-supported amorphous BaO overlayer that forms at intermediate Ba loadings of ~6–12 wt% provides an optimum morphology for NO_x uptake.

Acknowledgements

This work was supported by the U.S. Department of Energy's (DOE) Office of Science, Basic Energy Sciences, Division of Chemical Sciences, Biosciences and Geosciences, by the DOE's Office of Energy Efficiency and Renewable Energy, Vehicle Technologies Program, and by a Laboratory Directed Research and Development (LDRD) project at Pacific Northwest National Laboratory (PNNL). Computing time was granted by the National Energy Research Scientific Computing Center (NERSC) under project no. m752. A portion of the computing time was also granted by the scientific user project (st30469) using the Molecular Science Computing Facility in the William R. Wiley Environmental Molecular Sciences Laboratory (EMSL). The EMSL is a DOE national scientific user facility located at PNNL, and supported by the DOE's Office of Science, Biological and Environmental Research.

References

[1] W.S. Epling, L.E. Campbell, A. Yezerets, N.W. Currier, J.E. Parks, Catal. Rev. 46 (2004) 163.
[2] S. Roy, A. Baiker, Chem. Rev. 109 (2009) 4054.
[3] W.S. Epling, C.H.F. Peden, J. Szanyi, J. Phys. Chem. C 112 (2008) 10952.
[4] F. Frola, M. Manzoli, F. Prinetto, G. Ghiotti, L. Castoldi, L. Lietti, J. Phys. Chem. C 112 (2008) 12869.
[5] A. Desikusumastuti, M. Laurin, M. Happel, Z. Qin, S. Shaikhutdinov, J. Libuda, Catal. Lett. 121 (2008) 311.
[6] C.W. Yi, J. Szanyi, J. Phys. Chem. C 113 (2009) 2134.
[7] C.W. Yi, J. Szanyi, J. Phys. Chem. C 113 (2009) 716.
[8] J. Szanyi, J.H. Kwak, J. Hanson, C.M. Wang, T. Szailer, C.H.F. Peden, J. Phys. Chem. B 109 (2005) 7339.
[9] J.H. Kwak, D.H. Mei, C.W. Yi, D.H. Kim, C.H.F. Peden, L.F. Allard, J. Szanyi, J. Catal. 261 (2009) 17.
[10] C.W. Yi, J.H. Kwak, C.H.F. Peden, C.M. Wang, J. Szanyi, J. Phys. Chem. C 111 (2007) 14942.
[11] J. Szanyi, J.H. Kwak, D.H. Kim, S.D. Burton, C.H.F. Peden, J. Phys. Chem. B 109 (2005) 27.
[12] P. Broqvist, H. Gronbeck, E. Fridell, I. Panas, Catal. Today 96 (2004) 71.
[13] P. Broqvist, H. Gronbeck, E. Fridell, I. Panas, J. Phys. Chem. B 108 (2004) 3523.
[14] P. Broqvist, I. Panas, E. Fridell, H. Persson, J. Phys. Chem. B 106 (2002) 137.
[15] P. Broqvist, I. Panas, H. Gronbeck, J. Phys. Chem. B 109 (2005) 15410.
[16] L. Cheng, Q.F. Ge, Surf. Sci. 601 (2007) L65.
[17] L. Cheng, Q.F. Ge, J. Phys. Chem. C 112 (2008) 16924.
[18] E.J. Karlsen, M.A. Nygren, L.G.M. Pettersson, J. Phys. Chem. B 107 (2003) 7795.
[19] D.H. Mei, Q.F. Ge, J.H. Kwak, D.H. Kim, C. Verrier, J. Szanyi, C.H.F. Peden, Phys. Chem. Chem. Phys. 11 (2009) 3380.
[20] W.F. Schneider, J. Phys. Chem. B 108 (2004) 273.
[21] M.M. Branda, C. Di Valentin, G. Pacchioni, J. Phys. Chem. B 108 (2004) 4752.
[22] H. Gronbeck, P. Broqvist, I. Panas, Surf. Sci. 600 (2006) 403.
[23] V.E. Henrich, P.A. Cox, The Surface Science of Metal Oxides, Cambridge University Press, Cambridge, UK, 1994.
[24] W.F. Schneider, K.C. Hass, M. Miletic, J.L. Gland, J. Phys. Chem. B 106 (2002) 7405.
[25] D. Mei, Q.F. Ge, J. Szanyi, C.H.F. Peden, J. Phys. Chem. C 113 (2009) 7779.
[26] G. Kresse, J. Furthmuller, Phys. Rev. B 54 (1996) 11169.
[27] G. Kresse, J. Furthmuller, Comput. Mater. Sci. 6 (1996) 15.
[28] P.E. Blochl, Phys. Rev. B 50 (1994) 17953.
[29] G. Kresse, D. Joubert, Phys. Rev. B 59 (1999) 1758.
[30] J.P. Perdew, K. Burke, M. Ernzerhof, Phys. Rev. Lett. 77 (1996) 3865.
[31] J.H. Kwak, J.Z. Hu, D.H. Kim, J. Szanyi, C.H.F. Peden, J. Catal. 251 (2007) 189.
[32] D.H. Mei, Q.F. Ge, J.H. Kwak, D.H. Kim, J. Szanyi, C.H.F. Peden, J. Phys. Chem. C 112 (2008) 18050.
[33] J.H. Kwak, J.Z. Hu, D.H. Mei, C.W. Yi, D.H. Kim, C.H.F. Peden, L.F. Allard, J. Szanyi, Science 325 (2009) 1670.
[34] R.F.W. Bader, Acc. Chem. Res. 18 (1985) 9.
[35] G. Henkelman, A. Arnaldsson, H. Jonsson, Comput. Mater. Sci. 36 (2006) 354.
[36] A. Desikusumastuti, T. Staudt, M. Happel, M. Laurin, J. Libuda, J. Catal. 260 (2008) 315.
[37] W.S. Epling, J.E. Parks, G.C. Campbell, A. Yezerets, N.W. Currier, L.E. Campbell, Catal. Today 96 (2004) 21.
[38] N.W. Cant, M.J. Patterson, Catal. Today 73 (2002) 271.
[39] I. Nova, L. Castoldi, L. Lietti, E. Tronconi, P. Forzatti, F. Prinetto, G. Ghiotti, J. Catal. 222 (2004) 377.